Chapter 2
The Sun as Power Source for Spaceflight

In-Space Use of the Continuous Sunlight Pressure If we were in the pre-IKAROS scenarios of space sailing, the main aim of this chapter would be to show that one *may* utilize the radiant energy from the Sun as external-to-spacecraft source of thrust. Now, as the Japanese sail-based spacecraft proved that solar sailing is a reality (even though at the level of orbit perturbation, for the moment), this chapter aims at discussing more in detail the principles of sunlight utilization for efficacious in-space propulsion.

We start with a summary of radiometric quantities, and then we point out the immense contribution of space-era to the solar physics, in particular through the high-precision records of the total and spectral solar irradiances. The time series of such quantities will be important in designing fast solar-sail trajectories. In particular, we highlight the principles of utilization of the solar irradiance for in-space propulsion.

2.1 A Summary of Radiometric Quantities

In this section, we expound on radiometric quantities involved in space trajectories, when the radiation pressure produces either the main thrust acceleration or a perturbing acceleration, as in many real situations. Radiometry is standardized by the Commission Internationale de L'Eclairage (CIE), or International Commission on Illumination, International Standards Organization (ISO), and International Union of Pure and Applied Physics (IUPAP).

Radiometry is the science aiming at measuring physical quantities relevant to electro-magnetic (e.m.) radiation, in principle from radio waves to γ-rays. However, in practice, one often refers to as radiometry in the context of infrared, visible and ultraviolet bands of the e.m. spectrum. By saying that, one implicitly assumes that light is viewed as classical waves, not as quantum objects—the photons—though a net separation is neither possible nor required for propulsion purposes. The twofold amazing nature of light is well known; however, some further clarification is necessary in the framework of this book. Going straight to the problem's core, for a

G. Vulpetti, *Fast Solar Sailing*, Space Technology Library 30,
DOI 10.1007/978-94-007-4777-7_2,

general photon-induced space sailing (i.e. not only solar-photon sailing), we need light incident on some (sufficiently large) spacecraft's surface (the *sail*), and emerging from it after having interacted with the sail's material. Well, we can picture both incident and reflected light *classically*, namely, as the full wave theory states. However, the photon-surface interaction should be modeled by treating the material's atoms and molecules as quantum objects. Even in this semi-classical approach, things look somewhat complicated, and so they are indeed. In-space propulsion needs high flows or streams of photons because radiation pressure has to be transformed into sufficiently high thrust.

If we utilized a single-mode-operated laser, with a given frequency and well above the threshold, for pushing a sail, then the photon statistics of this light would be close to a Poissonian inasmuch as this operational type of lasing is a good approximation to perfectly coherent light, which obeys the Poisson distribution.

In general, the statistics describing the fluctuations of the number of photons from a *single-mode* of the radiation field is known as the Bose-Einstein distribution (BE). Let us consider *thermal light*, namely, the light emitted from a blackbody. A single mode of thermal light is super-Poissonian (i.e. the variance is higher than the mean). However, blackbody light has a continuum of modes. As a result, the statistics of it exhibits a Poissonian character, as measured in many experiments. As a point of fact, the super-Poissonian variance tends to become Poissonian if the number of modes is high.

Quantum optics re-interprets the usual energy expression of the quantum harmonic oscillator in the n-state, namely, $E_n = (\frac{1}{2} + n)\hbar\omega$ as n photons *excited* at angular frequency ω. The very quantum nature of light can be detected in special experiments where photon statistics is sub-Poissonian [13] (i.e. the variance is lower than the mean). Beams of light can be classified not only with respect to the photon statistics, but also via the second-order correlation function, which quantifies the time fluctuations of intensity. In other words, there may be streams of light (the so-called *antibunched* light), where the photons are "separated" by regular gaps.

Sunlight originates from a stellar atmosphere with different brightness temperatures (as we will see later in this chapter); it is, as a whole, a classical electromagnetic radiation delivering pressure. (Where appropriate, we will view sunlight as photons with energy and momentum). The practical consequence of these facts is that macroscopic **radiometric** quantities represent an appropriate tool for dealing with the generation of radiation-pressure thrust, a topic that shall be developed in many details in Chap. 6.

Like radiometry, *photometry* regards measurements of electromagnetic radiation, but that one detectable by the human eye. Quantitatively, a photometric quantity is strongly affected by the eye's spectral sensitivity, which is restricted from 380 nm to

800 nm, approximately, in wavelength. Although human eye exhibits photopic vision, mesopic vision, and scotopic vision, CIE's spectral luminous efficiency function regards the eye's average response under daylight conditions. When the behavior of the human eye under dark-adapted conditions (or also in intermediate lighting conditions) becomes important for some measurable quantity, one will replace the photopic function by the scotopic (mesopic) sensitivity function. We are not concerned with photometry here since a solar, laser, or microwave sail can be viewed as a special detector of e.m. radiation as a device utilizing the pressure of light, and in a range well wider than the human eye's.

Now, we can list and briefly comment on some radiometric definitions. The list is incomplete; fundamental radiometric functions are to be defined in Chap. 6 where we shall model the solar-sail thrust. Here, for each concept, *spectral*-quantity is stated first, then the *integral* one will follow. We will make only a few changes in symbols, but **not** in concepts, with respect to the international standard. Units follow strictly the International System of Units (SI). Each item is arranged as follows: quantity name, symbol, units, definition, and comments (if any).

- **Source of Light**: a source of electromagnetic radiation can be the surface of a proper photon emitter (e.g., stars, lamps, gases, plasmas, living bodies, etc.) or any surface reflecting/scattering some fraction of the received light. When the source does not appear as point-like to some observer, it can be partitioned in infinitesimal, or differential, surfaces, each of which is endowed generally with its own radiation characteristics.
- Let $\mathrm{d}\mathbf{A}$ be a differential *directed* surface,[1] which emits or receives electromagnetic energy. Let also $\mathbf{n}$ be the positive normal to $\mathrm{d}\mathbf{A}$. A direction $\mathbf{d}$, along which radiation can be emitted or received, forms an angle θ with $\mathbf{n}$; $\mathrm{d}\omega$ denotes the solid angle about $\mathbf{d}$. Then, the orthogonal-to-$\mathbf{d}$, or *projected*, area is equal to $\mathrm{d}A_{\perp} = \cos\theta\,\mathrm{d}A$, where $\mathrm{d}A$ denotes the magnitude of $\mathrm{d}\mathbf{A}$. Note that an infinitesimal surface may be a pure geometric object *across* which light can go. In any case, light is assumed to impinge on or leave a surface element in the semi-space containing *its* $\mathbf{n}$.

  The concepts we are discussing have to be eventually applied to real-life surface elements. Each element will be sufficiently small to be dealt mathematically with as infinitesimal area, but also sufficiently large to contain a high number of atoms/molecules, and to exhibit two sides that may have some different optical properties.

- **Spectral Radiant Power** or spectral radiant **Flux** (Φ_λ, $\mathrm{W\,nm^{-1}}$). Let $\mathrm{d}^2Q(t,\lambda)$ denote the amount of electromagnetic energy (as established via Maxwell equations) that stems from a source of light in the wavelength band $[\lambda, \lambda + \mathrm{d}\lambda]$ and during the interval $[t, t + \mathrm{d}t]$. According to the two previous definitions, such elemental energy may be emitted by the surface of any real *active* body, reflected/diffused by, or transmitted across any real surface, or may "impinge" upon

[1] In the language of geometric algebra, $\mathrm{d}\mathbf{A}$ is a bivector.

a purely geometrical surface. The following expression defines the spectral radiant power

$$\Phi_\lambda = \frac{\mathrm{d}^2 Q(t,\lambda)}{\mathrm{d}\lambda\,\mathrm{d}t} \tag{2.1}$$

where function $Q(t,\lambda)$ is supposed differentiable with respect to t and λ.[2]

- **Radiant Power** or radiant **Flux** (Φ, W) is the spectral radiant power integrated over the full wavelength spectrum

$$\Phi(t) = \int_0^\infty \Phi_\lambda\,\mathrm{d}\lambda \tag{2.2}$$

In practice, the integral (2.2) is restricted from some $\lambda_1 > 0$ to some finite $\lambda_2 > \lambda_1$. Though it may be a time-valued function peculiar to the emitting body, normally Φ contains no other source-related information.

However, both radiant-power concepts can be extended to emitting/receiving surface and solid angle about a propagation direction based on d**A**; for instance, one could mean

$$\Phi = \Phi(t,\lambda,A,\omega) \tag{2.3}$$

for a more general function of *independent* variables to be used in additional radiometric definitions, as shown below.

- **Spectral Radiant Exitance** (M_λ, $\mathrm{W\,nm^{-1}\,m^{-2}}$) is the spectral radiant power emitted per source's unit area

$$\mathrm{M}_\lambda = \mathrm{d}\Phi_\lambda/\mathrm{d}A = \mathrm{d}^2\Phi/\mathrm{d}\lambda\,\mathrm{d}A \tag{2.4}$$

- **Radiant Exitance** (M, $\mathrm{W\,m^{-2}}$) is the spectral radiant exitance integrated over the full wavelength spectrum

$$\mathrm{M} = \int_0^\infty \mathrm{M}_\lambda\,\mathrm{d}\lambda \tag{2.5}$$

In practice, the integral (2.5) extends from some $\lambda_1 > 0$ to some finite $\lambda_2 > \lambda_1$.

- **Spectral Radiant Intensity** (F_λ, $\mathrm{W\,nm^{-1}\,sr^{-1}}$) is the spectral power, per unit solid angle, emitted by a radiation source. By definition one writes

$$\mathrm{F}_\lambda = \mathrm{d}\Phi_\lambda/\mathrm{d}\omega = \mathrm{d}^2\Phi/\mathrm{d}\lambda\,\mathrm{d}\omega \tag{2.6}$$

where $\mathrm{d}\omega$ is an infinitesimal solid angle about the direction **d** from d**A**. Therefore, additional information regards the angular distribution of the source's spectral

[2] In the framework of this book, such assumption is always satisfied.

power. Spectral intensity and spectral exitance are interrelated by the following equation:

$$\mathrm{F}_\lambda \, \mathrm{d}\omega = \mathrm{M}_\lambda \, \mathrm{d}A \tag{2.7}$$

which follows from (2.6) and (2.4).

- **Radiant Intensity** (F, $\mathrm{W\,sr^{-1}}$) is the source's spectral radiant intensity integrated over the full wavelength spectrum

$$\mathrm{F} = \int_0^\infty \mathrm{F}_\lambda \, \mathrm{d}\lambda \tag{2.8}$$

In practice, the integral (2.8) extends from some $\lambda_1 > 0$ to some finite $\lambda_2 > \lambda_1$.

- **Spectral Radiance** (L_λ, $\mathrm{W\,nm^{-1}\,sr^{-1}\,m^{-2}}$) is the spectral power, per unit solid angle and per unit *projected* area, emitted by a radiation source. In formulas,

$$\mathrm{L}_\lambda = \mathrm{d}^3\Phi / \mathrm{d}\lambda \, \mathrm{d}\omega \, \mathrm{d}A_\perp = \mathrm{d}F_\lambda / \mathrm{d}A_\perp \tag{2.9}$$

This radiometric quantity contains information about power distribution as function of the emitting area element, emission direction, and wavelength at some time t.

- **Radiance** (L, $\mathrm{W\,sr^{-1}\,m^{-2}}$) is the spectral radiance integrated over the full wavelength spectrum

$$L = \int_0^\infty \mathrm{L}_\lambda \, \mathrm{d}\lambda \tag{2.10}$$

In practice, the integral (2.10) extends from some $\lambda_1 > 0$ to some finite $\lambda_2 > \lambda_1$. We then have a *broadband* radiance.

- **Spectral Irradiance** (I_λ, $\mathrm{W\,nm^{-1}\,m^{-2}}$) is the spectral radiant power incident on or crossing a surface of unit area; this power can come from any direction in the semispace containing **n** according to the above convention, in particular from a finite number of single directions simultaneously:

$$\mathrm{I}_\lambda = \mathrm{d}\Psi_\lambda / \mathrm{d}A \tag{2.11}$$

where Ψ_λ denotes the spectral power arriving at $\mathrm{d}\mathbf{A}$.

- **Irradiance** (I, $\mathrm{W\,m^{-2}}$) is the spectral irradiance integrated over the full wavelength spectrum

$$\mathrm{I} = \int_0^\infty \mathrm{I}_\lambda \, \mathrm{d}\lambda \tag{2.12}$$

In practice, the integral (2.12) is restricted from some $\lambda_1 > 0$ to some finite $\lambda_2 > \lambda_1$. We then have a *broadband* irradiance. One should note that the cosine law is automatically taken into account in computing the total rate of energy deposited on $\mathrm{d}A$ from different directions. Therefore, if one or more light's beams arrive orthogonally to the considered surface, total irradiance is at its maximum. Spectral irradiance should not be confused with spectral intensity.

We have discussed radiometric functions starting from the concept of infinitesimal radiant energy, and radiant power has been defined for the first. As a point of fact, normally is power (not energy) involved in the characterization of a source of light (in the general sense explained above).

Definitions of the radiometric quantities do not mention any relative motion between surfaces which emit/receive/transmit electromagnetic radiation. They implicitly refer to some frame attached to the considered surface. However, when one deals with at least one energy source and at least one receiving surface, aberration of light can, for example, no longer be neglected if their relative velocity is sufficiently high.

Some further notes about the above definitions are in order.

1. Normally, the adjective *radiant* may be suppressed during statements, sentences etc, when no ambiguity is generated since the sole energy form in the context is the radiant one.
2. Both (spectral) exitance and (spectral) irradiance can be grouped conceptually into (spectral) *flux density*, but with the distinction between the 'leaving from' and 'the arriving at' possibilities, respectively.
3. Depending on the problem at hand, either wave frequency or energy may be used instead of wavelength.
4. Although many international efforts to achieve a world-wide standard in defining radiometric quantities, however some scientific communities prefer to have their own definitions. The problem is that some words refer to different concepts. One of the terms causing confusion is *intensity*, often referred to as power per unit solid angle or power per unit area. Another term of misunderstanding is *flux* sometimes used as shorthand for flux density. The two terms have different meanings and should *not* be interchanged. Thus, one should be particularly careful when comparing results coming from documents issued by different scientific communities.

The concept of completely isotropic source of light implies a spherical source whose *intensity* is direction independent. A distant star can be considered an isotropic and point-like source from our vantage points in the solar system. Not so the Sun, as we shall see in the next section.

A flat radiating surface, either active or passive, may in principle exhibit a *radiance* independent of the emission direction over its whole hemisphere. Such an ideal surface is called Lambertian. If the surface is passive, uniform diffusion of light takes place. The concept is applicable to each of the differential areas in which a finite curved surface can be partitioned. It's easy to show that the exitance of a Lambertian surface, either infinitesimal or finite, is related to its radiance via a simple but meaningful relationship:

$$\mathrm{M} = \pi \mathrm{L} \tag{2.13}$$

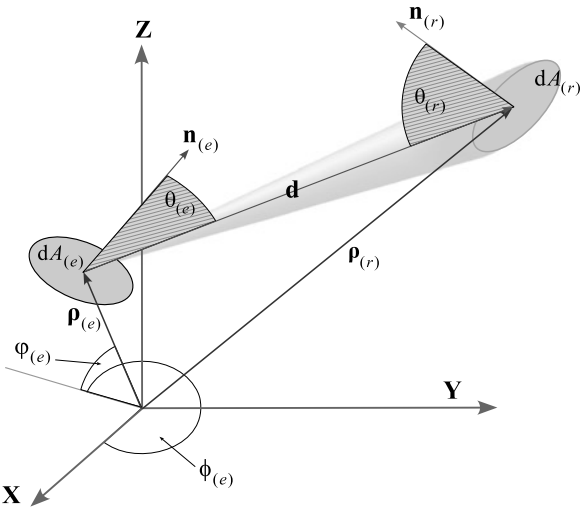

Fig. 2.1 Geometry of an infinitesimal surface receiving radiation from an infinitesimal source

The factor π steradians comes from the definition of radiance that relies on the area projected along a given direction. A Lambertian surface is also known as the ideal diffuser. A blackbody radiator is Lambertian as well. In Chap. 6, we will analyze the blackbody sail.

Now let us work out the irradiance of an elemental surface brought about by the radiance of an infinitesimal emitting surface. This will be useful in other chapters for setting the algorithm giving the solar irradiance onto an arbitrary oriented sail at an arbitrary distance from the Sun. Figure 2.1 shows the geometry we are using; subscripts (e) and (r) refer to as the emitting and receiving areas, respectively. One has

$$\mathbf{d} = \boldsymbol{\rho}_{(r)} - \boldsymbol{\rho}_{(e)}, \qquad \|\mathbf{d}\| \equiv d \tag{2.14a}$$

$$\cos\theta_{(e)} = \mathbf{n}_{(e)} \cdot \mathbf{d}/d, \qquad \cos\theta_{(r)} = -\mathbf{n}_{(r)} \cdot \mathbf{d}/d \tag{2.14b}$$

$$\cos\theta_{(e)} \geq 0, \qquad \cos\theta_{(r)} \geq 0 \tag{2.14c}$$

The differential power received from the surface of area $\mathrm{d}A_{(r)}$ can be expressed as

$$\begin{aligned} \mathrm{d}^2\Phi_{(r)} &= \mathrm{L}_{(e)}\,\mathrm{d}A_{(e)}\cos\theta_{(e)}\,\mathrm{d}\omega_{(r)} \\ &= \mathrm{L}_{(e)}\,\mathrm{d}A_{(e)}\cos\theta_{(e)}\frac{\mathrm{d}A_{(r)}\cos\theta_{(r)}}{d^2} \end{aligned} \tag{2.15}$$

Therefore, from the definition of irradiance and (2.15), the irradiance onto the passive area element results in

$$\mathrm{dI}_{(r)} = \frac{\mathrm{d}^2\Phi_{(r)}}{\mathrm{d}A_{(r)}} = \mathrm{L}_{(e)}\cos\theta_{(e)}\cos\theta_{(r)}d^{-2}\,\mathrm{d}A_{(e)} \tag{2.16}$$

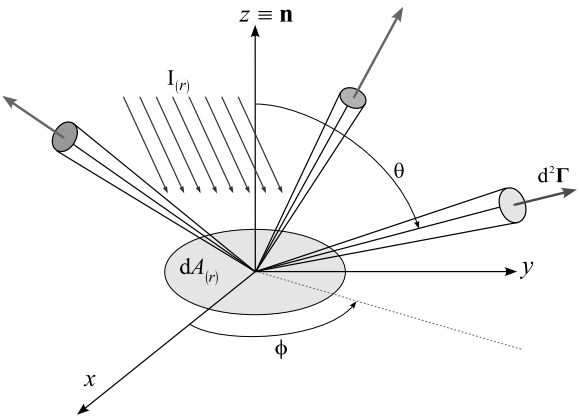

Fig. 2.2 Light's diffusion momenta: the z-axis of the reference frame is along the normal to the surface element. In general, each differential solid angle hosts a different 2nd-order momentum rate $\mathrm{d}^2\mathbf{\Gamma}$ of leaving light, as indicated by different-length arrows

Inequalities in (2.14a), (2.14b), normally taken for granted, mean that the receiving and the emitting surfaces can see one another *directly*. The second (or back) *side* of a passive real surface can see the radiating surface indirectly, namely, via some reflection(s) (of the emitted light) from other surfaces, or (partial or total) transmission of light through the first (or front) side: for example, an arbitrary (concave or convex) finite surface radiating energy onto another arbitrary (concave or convex) finite surface. Things are still more complicated when either the emitting or the receiving surface, or both, change their orientation in space. Furthermore, the source of e.m. radiation may be a hot plasma that the receiving surface sees at different depths. Whereas (2.16) holds in general, its integral in various real configurations can be complicated to evaluate, even numerically.

Now, let us introduce the concept of coefficient of diffuse momentum[3] related to a surface that scatters light. We will use the same area element labeled by (r) in Fig. 2.1. Let us suppose to know the irradiance onto the area $\mathrm{d}A_{(r)}$ coming from one (arbitrary) direction and *scattering* in the same hemisphere (as shown in Fig. 2.2); we are referring to the bidirectional-reflection function, detailed in Sect. 6.4.2.

The 2nd-order momentum rate $\mathrm{d}^2\mathbf{\Gamma}$, associated to the reflected radiance in the direction (ϕ, θ), can be expressed by

$$\mathrm{d}^2\mathbf{\Gamma}_{(re)} = \frac{\mathrm{L}_{(re)}(\phi, \theta)}{c}\, \mathrm{d}A_{(r)} \cos\theta \begin{pmatrix} \sin\theta\cos\phi \\ \sin\theta\sin\phi \\ \cos\theta \end{pmatrix} \mathrm{d}\omega \tag{2.17}$$

where the subscript (re) refers to reflection, and we have emphasized the fact that the radiance from $\mathrm{d}A_{(r)}$ is not isotropic, in general; (this concept will be made more precise in Chap. 6). As a result, the direction of the integrated momentum rate can be different from either $\mathbf{n} = (0\ 0\ 1)^\top$ or the specular-reflection direction. If we focus

[3] This one should not be confused with the coefficients related to particle diffusion in gas or plasma.

on the total momentum rate due to *diffuse* reflection, then we have formally

$$\mathrm{d}\boldsymbol{\Gamma}_{(diff)} = \int_{2\pi\ \mathrm{sr}} \mathrm{d}^2\boldsymbol{\Gamma}_{(diff)} \tag{2.18}$$

Let us note that the scattered exitance from the considered surface can be written

$$\mathrm{M}_{(re)}\,\mathrm{d}A_{(r)} = \mathrm{d}\Phi_{(re)} = (\mathcal{R}_{(diff)} + \mathcal{R}_{(spec)})\mathrm{I}_{(r)}\,\mathrm{d}A_{(r)} \equiv \mathcal{R}\mathrm{I}_{(r)}\,\mathrm{d}A_{(r)} \tag{2.19}$$

$\mathcal{R}_{(diff)}$ denoting the diffuse reflectance of the surface, namely, the fraction of the received energy that is reflected diffusely, whereas $\mathcal{R}_{(spec)}$ is the specular fraction. The coefficient of diffuse momentum is defined as follows

$$\chi = \frac{\|\mathrm{d}\boldsymbol{\Gamma}_{(diff)}\|/\mathrm{d}A_{(r)}}{\mathrm{M}_{(diff)}/c} = \frac{\|\mathrm{d}\boldsymbol{\Gamma}_{(diff)}\|/\mathrm{d}A_{(r)}}{(\mathcal{R}_{(diff)}/\mathcal{R})\mathrm{M}_{(re)}/c} \tag{2.20}$$

In this ratio, the numerator represents the radiation pressure associated with the vector sum of the diffuse momenta, whereas the denominator is the pressure that one would get if the diffuse exitance were turned into a directional beam. If one deals with a Lambertian surface, i.e. $\mathrm{L}_{(diff)} = \mathrm{L}_{(re)} \equiv \mathrm{L}^{(\mathfrak{L})} = \mathrm{M}^{(\mathfrak{L})}/\pi = \mathrm{M}_{(re)}/\pi = \mathrm{M}_{(diff)}/\pi$, then the integration of (2.17) with respect to ϕ and θ becomes easy and produces

$$\mathrm{d}\boldsymbol{\Gamma}^{(\mathfrak{L})} = \frac{\mathrm{L}^{(\mathfrak{L})}}{c}\,\mathrm{d}A_{(r)} \begin{pmatrix} 0 \\ 0 \\ 2\pi/3 \end{pmatrix} \tag{2.21}$$

where the superscript $(\mathfrak{L})$ denotes a Lambertian-surface quantity. As a result, $\chi^{(\mathfrak{L})} = 2/3$. Although not strictly, χ-deviations from such values may be interpreted as non-Lambertian behaviors. The usefulness of the coefficient of diffuse momentum comes from modeling the recoil thrust due to the scattering of light from a surface (Chap. 6), in particular a solar sail. In simple models with paraxial solar incidence, the diffuse-reflection thrust component is assumed directed along the surface normal and with a magnitude proportional to $\chi\mathcal{R}_{diff}$. In a quite similar way, one can define coefficients of diffuse-transmittance momentum. In Chap. 6, we will be concerned with models based on complicated diffraction theories and mathematical descriptions of real-surfaces.

2.2 Monitoring Sunlight from Satellite

In this section, we will describe features of the solar irradiance that are of particular relevance to the sailcraft dynamics and design. From chosen references of the specialized literature on solar irradiance and models of the solar photosphere, and the close atmospheric layers, we will recall a few items about the current knowledge of the Sun, but only for a more fluent description of what is of matter for solar sailing, in general, and fast sailing, in particular. We begin with mentioning the revolution

in the measurements of solar irradiance started in 1978. Then, we will discuss about total and spectral solar irradiances in two separate subsections. Finally, in Sect. 2.3, we will draw some indications relevant to sailcraft trajectory and solar-sail design.

In building a standard in solar spectral irradiance, e.g. the tables in [3] from 0.1195 to 1,000 μm, not only measurements from spacecraft have been extensively employed, but also many, many observational data from high-altitude aircraft and ground devices; also, solar-irradiance models have been taken into account.

Before the beginning of the astronautical era, there was no universally-accepted evidence that the so-called *solar constant* might vary from a strict constant value. Ground measurements *sufficiently* accurate/precise to reveal any real deviation from a constant value were not possible, in practice, before space satellites (e.g. [6, 18]). Many historical ideas, concepts, and facts (from China, Europe, and United States) about the Sun and analyses of the solar objects affecting the Sun's electro-magnetic emission can be found in [32]. After the first direct measurements of sunlight carried out by padre A. Secchi (Vatican State) and the studies of S. P. Langley (USA) in the 19th century, C. G. Abbot (USA) was a pioneer in measuring the solar constant and its claimed variability for decades [1]. However, such measurements (though carried out from observation stations on mountains of United States, Chile, and Arabia, and by means of new instruments) indicated a too much high (some percent) solar change. A remarkable synopsis of his and his team's measurement campaigns are described in [2].

On November 16, 1978, the first cavity radiometer, named HF after Hickey-Frieden, was switched on aboard the U.S. satellite NIMBUS-7; this was followed by other satellites endowed with modern instruments for observing the Sun. One of the most striking results of the space era has been the discovery that the Total Solar Irradiance (TSI) (standardized at 1 AU) is variable indeed. Let us be a bit more precise: in the Hertzsprung-Russell diagram (HR), the plot of star's luminosity[4] *vs* star's surface blackbody temperature, each star occupies a dot. A main-sequence star like the Sun stays fixed in the diagram for a time ranging from hundred millions to billions of years, depending non-linearly and inversely on the star mass.

However, the extended measurement campaigns, started on November 1978, have been confirming that the Sun is a *variable* star, and new knowledge—also through advanced solar dynamo models—have been accumulated in the last three solar cycles (21–23), and is continuing in the cycle-24. (Sunspot cycles are counted conventionally from the cycle in the period 1755.03-1766.06, or the solar cycle 1).

Before going on, we have to clarify that, from an astrophysical viewpoint, the Sun is still a fixed-luminosity star because its variations with time are

[4]This is the radiant power emitted by a star.

rather small. A variable star, in the astrophysical sense, is something of much different from and stronger than the Sun (e.g. Cepheid-type stars). Nevertheless, the actual small changes of the TSI are capable to affect the Earth's climate evolution in the long run, even though in the last decades the anthropogenic actions on climate have been becoming stronger and stronger, according to the Intergovernmental Panel on Climate Change (IPCC) of the United Nations.

In order to better grasp how and how much the solar-irradiance campaigns have so positively affected the current knowledge of the Sun, down here we will summarize the main instruments on some launched Sun-relevant satellites. We have arranged the main features by means of concise card-like information. Some pieces of information are related to the time of this writing.

Spacecraft: **NIMBUS-7** (launched in 1978)

- Experiment(s)/Instrument(s): Many experiments for Earth weather and total solar irradiance. Solar irradiance was measured by Hickey-Frieden (HF) radiometer.

NIMBUS-7 was the last of the NIMBUS-series of US satellites in Sun-synchronous orbits. The Hickey-Frieden cavity radiometer started measuring in November 1978. This type of radiometer replaced flat radiometers working on board former NIMBUS satellites.

Spacecraft: **Solar and Heliospheric Observatory (SOHO)** (launched in 1995)

- Experiment(s)/Instrument(s): Variability Irradiance Gravity Oscillation (VIRGO):
- measurements of total solar irradiance by two high-accuracy two-cavity differential absolute radiometers (DIARAD and PM06V)
- Monitoring of the solar spectral irradiance at 402, 500 and 862 nm with a 3-channel sun photometer
- Spectral radiance at 500 nm with a luminosity oscillation imager
- Continuous high-precision, high-stability and high-accuracy measurements of the solar total and spectral irradiance, and spectral radiance variation; long-term precision of the time series from VIRGO resulted in about 2 ppm/year ($1\,\sigma$)
- Experiment(s)/Instrument(s): Solar Ultraviolet Measurement of Emitted Radiation (SUMER):
- Spectrograph operating in either spectral scan (80–150 nm, 1024 pixels) or raster scan (360 spatial pixels), spatial resolution 1 arc-second (i.e. about 730 km on the Sun)

SOHO has been operating in a halo orbit about the (Lagrange) L1 point of the Sun-Earth gravitational system (about 1.5 million kilometers from Earth towards the Sun). Two absolute radiometers are onboard. This has been quite important in comparing and reconstructing data of total solar irradiance.

Spacecraft: **ACRIMSAT** (launched in 1999)

- Experiment(s)/Instrument(s): Measurements of total solar irradiance via ACRIM-III

Instruments of the series Active Cavity Radiometer Irradiance Monitor (ACRIM) were put on various spacecraft designed for solar investigations. ACRIM-III, designed for NASA by the Jet Propulsion Laboratory, has continued to extend the database started with ACRIM I launched in 1980 on the Solar Maximum Mission (SMM) spacecraft. ACRIM II was on the Upper Atmosphere Research Satellite (UARS) launched in 1991. ACRIMSAT has operated in Sun-synchronous orbit.

Spacecraft: **ENVISAT** (launched in 2002)

- Experiment(s)/Instrument(s): Scanning Image Absorption Spectrometer for Atmospheric Cartography (SCIAMACHY)
- 240–2380 nm with resolution range from 0.2 to 1.5 nm (transmission, reflection, scattering of sunlight by either the Earth's atmosphere or surface)
- Experiment(s)/Instrument(s): Measurements of the Earth's reflectance (from surface and atmosphere) via Medium Resolution Imaging Spectrometer (MERIS):
- Earth's reflectance in the solar spectral range 390–1040 nm segmented in 15 spectral bands
- Experiment(s)/Instrument(s): Global Ozone Monitoring by Occultation of Stars (GOMOS)
- GOMOS looks to stars as they descend through the Earth's atmosphere and change color

ENVISAT, orbiting in a Sun-synchronous polar orbit, is completely oriented to radiation reflected by Earth, but data from it and other similar satellites are useful also to modeling radiation-pressure perturbations onto sailcraft spiraling about the Earth.

Spacecraft: **SORCE** (launched in 2003)

- Experiment(s)/Instrument(s): Total Irradiance Monitor (TIM), Spectral Irradiance Monitor (SIM), Solar Stellar Irradiance Comparison Experiment (SOLSTICE A, B)
- spectral range: 0.1–2400 nm (excluding the interval 40–115 nm)
- total-irradiance accuracy of 100 ppm with a long-term repeatability of 10 ppm/year
- daily measurements of the solar Ultraviolet (UV) irradiance in 120–300 nm with a spectral resolution of 1 nm; measurement accuracy less than 5 percent and long-term repeatability of 0.5 percent/year

SORCE (Solar Radiation and Climate Experiment) orbits about the Earth at an altitude of 640 km with 40° in inclination.

Spacecraft: **SDO** (launched February 11, 2010)

- Experiment(s)/Instrument(s): Atmospheric Imaging Assembly (AIA), Extreme ultraviolet Variability Experiment (EVE), Helioseismic and Magnetic Imager (HMI)
- AIA: Sun's images acquisition in 10 wavelengths every 10 seconds
- EVE/MEGS: multiple Extreme Ultraviolet (EUV) grating spectrograph (two Rowland-circle grating spectrographs) for spectral irradiance, operating in 0.1–7 nm (1-nm resolution), and 5–105 nm with (0.1-nm resolution)
- EVE/ESP: EUV Spectrometer (transmission grating spectrograph)
- HMI: continuous full-disk coverage at high spatial resolution

SDO (Solar Dynamics Observatory) is a 22-m^3 satellite with an initial mass of 3.2 tonne and has been designed for further understanding the Sun's influence on Earth and near-Earth space; it has been studying the solar atmosphere on small space and time scales, and in many wavelengths simultaneously. SDO is the first mission

for NASA's *Living With a Star* Program aimed at comprehending the causes of solar variability and its impacts on Earth. SDO circles Earth on an inclined geosynchronous orbit allowing for nearly-continuous and high data rate down to one dedicated ground station.

Spacecraft: **PICARD** (launched on June 15, 2010)

- Payload of PICARD consists of the following packages:
- SOVAP (SOlar VAriability PICARD): composed of a differential absolute radiometer and a bolometric sensor to measure TSI;
- PREMOS (PREcision MOnitor Sensor): a set of 3 photometers to study the ozone formation and destruction, helio-seismology, and 1 differential absolute radiometer for TSI;
- SODISM (SOlar Diameter Imager and Surface Mapper): an imaging telescope and a CCD aimed at measuring the solar diameter and shape with an accuracy of a few milli-arcsec; helio-seismological observations to probe the solar interior are also planned.

PICARD, from a French astronomer of 17th century, moves on a Sun-synchronous orbit at an altitude of 725 km.

2.2.1 The Total Solar Irradiance

This section is devoted to the discussion of some very notable results regarding the TSI measured in space. The panel-(a) of Fig. 2.3 shows the daily averages of the original TSI data coming from different radiometers, as described in Sect. 2.2, for solar observations from satellites: HF on spacecraft NIMBUS-7, ACRIM-I on SMM, ACRIM-II on UARS, either DIARAD or (DIARAD + PM06V = VIRGO) on SOHO, ACRIM-III on ACRIMSAT. (Data from TIM on SORCE have not be used in the construction of the following composites). Data in the same time intervals are dissimilar mainly for four reasons: different instrument characteristics, data acquisition interruption, different satellite attitudes, instrument degradation. Therefore, the (expected) problem arose from the need to compare the TSI time series coming from the various spacecraft in order to form a *composite* time series. Panels-(b,c,d) report the currently-available three composites named the PMOD, ACRIM, and IRMB composites, respectively, and covering three solar cycles, i.e. cycles 21–23. Such composites have been building in distinct ways: they use all the same original observational data-sets, but employ different procedures for removing sensitivity variations.

PMOD-composite is the only one which also corrects the early HF data for its degradation; in addition, it provides corrections to other satellite data (from HF and ERBS) available during the ACRIM's time gap (about 28 months) between the end of ACRIM-I operation and the begin of ACRIM-II campaign. The two other composites, similar to one another, do not include this correction procedure. The three composites are compared to the reconstruction of TSI from magnetograms and continuum images recorded at Kitt-Peak national observatory (USA/Arizona): the PMOD composite captures most of the variability variance, according to [11].

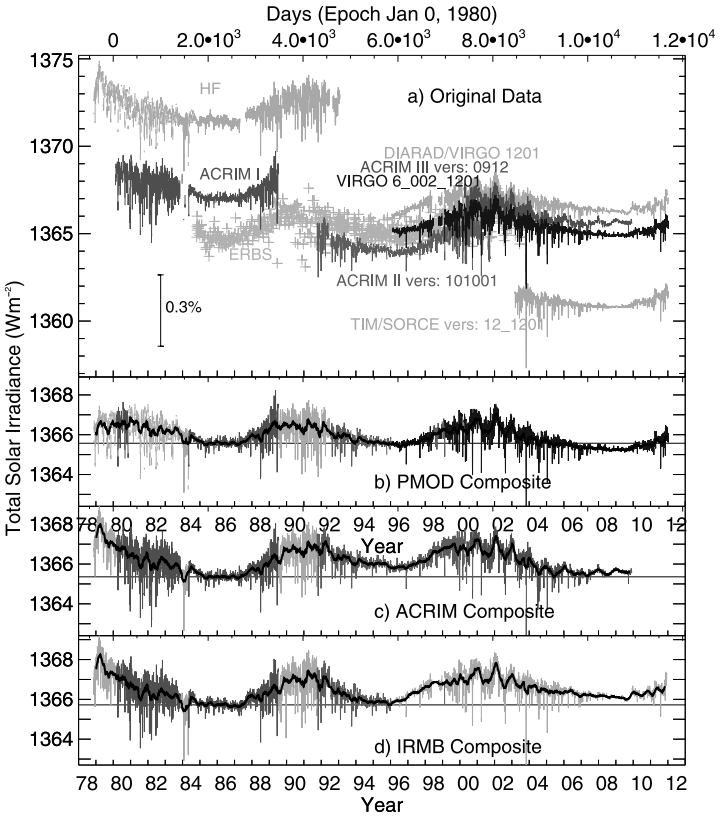

Fig. 2.3 Currently available composites of TSI since November 1978. They differ mainly on the considered satellite instruments and the way the raw data are corrected (Courtesy of C. Fröhlich, PMOD, World Radiation Center, Switzerland)

Figure 2.4 details the PMOD composite and reports additional information about the solar cycles 21–23; it marks the minima between two consecutive cycles. In particular, one can note that a proxy model [15], for explaining solar short and long-term behaviors during the last three cycles, has been successfully used for expanding the composite back to the cycle minimum occurred in 1976. Cycle-24 began in 2008.

Although highlighted at the beginning of Sect. 2.2 that—astrophysically speaking—the Sun has a constant radiant exitance, however it is notably variable for the solar system, in general, and for the Earth, in particular. Why is the Sun variable in TSI, though its variability is of the order of 0.1 percent (at least in the past decades)? Solar physicists have been advancing in explaining intrinsic phenomena in the upper layers of the solar atmosphere, in particular its "base" named the photosphere, a very useful picture of a spherical-like skin where astonishing phenomena take place.

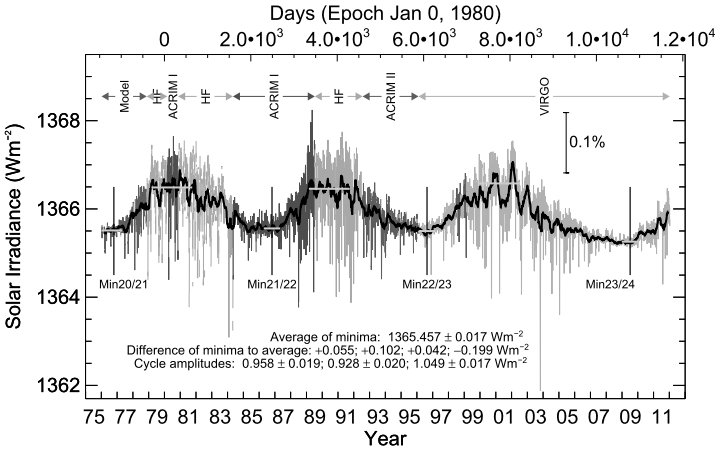

Fig. 2.4 Extended PMOD-Composite of Total Solar Irradiance. *Gray vertical segments* refer to the daily-means time series. Also reported are the differences between consecutive minima values, and the cycle amplitudes (Courtesy of C. Fröhlich, PMOD, World Radiation Center, Switzerland)

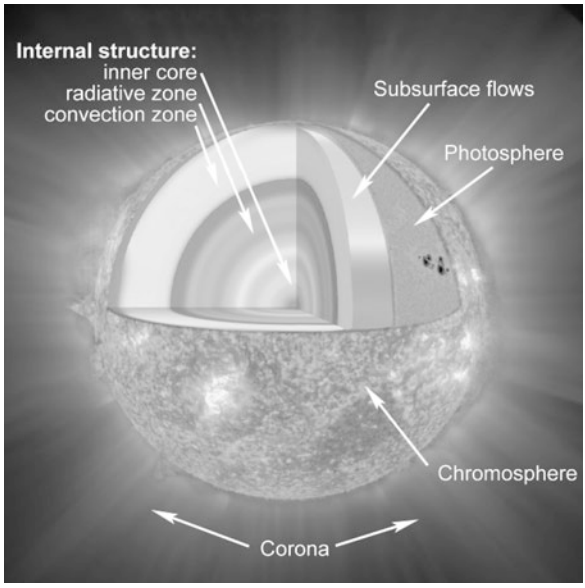

Fig. 2.5 Visualization of the solar structure via the shell concept (Courtesy of NASA)

Figure 2.5 shows a simplified shell model of the Sun. Substantially, the energy produced in the inner thermonuclear-reaction core (about $1/4$ of the solar radius $r_\odot$) diffuses outward by radiation (mainly γ and X-photons) through the radiative zone; the energy achieves the photosphere by fluid flows through the convection zone, extending in the last $0.3r_\odot$. Modern solar seismology has revealed a thin interface layer (not shown in the figure), called the *tachocline*, between the radiative zone

(with constant spin rate) and the differentially-rotating convection zone; it is where the Sun's magnetic field[5] is thought to be generated. There are different estimates of the tachocline thickness, depending essentially on the specific ways it is defined by; for example, some authors calculate $\delta_{tc}/r_{\odot} \cong 0.039$ at the solar equator, and 0.042 at 60° of heliographic latitude; other authors estimate $\delta_{tc}/r_{\odot}$ ranging from 0.016 to 0.038, whereas other evaluations are notably more different.

To have even a rough idea of how much dense is the Sun in the above-mentioned shells, we can mention that, from the innermost core to the photosphere, density varies of about nine orders of magnitudes. A better impressive quantity is perhaps the time the energy produced in the core (in a given time interval) takes to reach the photosphere: at least some thousands of years (someone estimates this energy travel lasting for a considerable fraction of a million years), instead of the ideal $r_{\odot}/c \sim 2$ s.

This concept of energy transport time should not be confused with the time the Sun would take to get rid of all energy stored in its inner core if the Hydrogen fusion stopped now: the Sun would remain luminous for at least twenty million years, but without producing neutrinos.

Above the photosphere, there is a thin layer (about one Earth diameter thick) named the chromosphere, more transparent than the photosphere in the visible band. It is significantly hotter than the photosphere. Chromosphere can be observed during total solar eclipses or by means of spectrographs with filters that isolate particular emitted lines, e.g. the H_{α} (reddish chromosphere) or the K-line (violet chromosphere) of the ionized Calcium atom. Above the chromosphere, separated by a thin and irregular layer named the transition region, one can find the *solar corona*, a very low density extended region of temperature rising to over a million (Kelvin) degrees. The corona can be observed by special instruments (the coronagraphs) or during total solar eclipses; it shines in X-rays, and considerably too, because of its high temperature. Both photosphere and chromosphere host a number of important features revealing the interaction of surface plasma elements with the magnetic field originated in the tachocline. One can observe a very rich fine structure in the continuum, spectral bands and spectral lines.

Useful is the concept of *quiet* Sun, applied particularly to the photosphere, which encompasses all the elements (ionized-gas and magnetic flux) *weakly* affected by the 11-year solar cycle. These elements may be grouped according to their horizontal scales in magnetic-flux tubes (a few hundred kilometers), granules and mesogranules (some thousand kilometers), and supergranules (greater than 10 thousand kilometers). Supergranules may be described as a pattern of irregular bright regions or cells of horizontal plasma outflows, covering the photosphere, known as the *supergranulation* (with a lifetime of about 1 day). The boundaries of supergranules are outlined by local magnetic features, or the photospheric *network*. The network exhibits high magnetic fields; in contrast, the interior of the network pattern is not magnetized (or above some low threshold). The quiet Sun structure is very spread

[5] In this and subsequent chapters, we use the custom term "magnetic field" for actually indicating the *magnetic induction field* or magnetic flux density, which is denoted by **B** and measured in Tesla, or $\mathrm{Wb/m^2}$, in the SI.

through the solar surface, so that its knowledge may be important for better understanding the photospheric magnetic evolution. Modern photosphere models, e.g. those ones considered in [21–25] and [30, 31], take a five-element typology into account: the Quiet Sun, sunspot umbrae, sunspot penumbrae, faculae, and the network. In addition to the network, sunspots and faculae are regions of high magnetic field, a typical sunspot extending in area much more than a facula. In the sunspot's darker core or umbra, the magnetic field is higher than in the peripheral regions or penumbra. Faculae appear notably brighter than sunspots, indicating higher temperatures of their magnetized plasma flows. Faculae are seen mainly at the limb of visible-band images of solar disk. Over them, images in the ionized Ca or H-α light show solar bright and large regions in the chromosphere, the *plages*.[6] During a typical sunspot cycle, faculae are usually close to sunspots; in period of intense magnetic activity, the area covered by both faculae and the (photospheric) network rises considerably. In addition, sunspot's mean-life is shorter than facula's, and sunspot "decays" into facula.

There is a more profound mechanism responsible for the fact that, when the number of sunspots increases, TSI increases (instead of decreasing as one would expect on sunspot basis only). This is explained in [11], and appears to be related to the local magnetic structure around sunspots and faculae, according to modern Magnetohydrodynamics (MHD) models. Very briefly, the sunspot darkness is ascribed to vertical and intense magnetic fields, which deflect the heat flow rising from deeper atmospheric zones. The blocked heat amount is not transferred or shunted nearby for re-emitting; instead, after horizontal diffusion, this energy flux goes back down rapidly into the Sun.

In contrast, faculae are bright because the magnetic field acts on smaller scales, and forms small depressions in the photosphere; thus, radiation from the hotter (because deeper) atmospheric layers is emitted with low attenuation.

Although not detectable in the periods of "classical" astronomy and astrophysics, namely, before the space era, however the fact that the net solar exitance can change should not surprise qualitatively too much once one considers the temperatures of the above-mentioned solar magnetic "objects". Figure 2.6 shows such temperatures versus the radial distance from the photosphere bottom. A big problem is to full understand quantitatively both short-time and secular trends in TSI variability (as also requested from many other areas of scientific investigation).

Observing the Sun radially from a sufficiently distant point in space (e.g. the Earth at 1 AU) at a chosen wavelength, the related optical depth $\tau(R)$ of such point can be set to zero. Then, one can define the *bottom* of the "solar surface" as the distance $r_\odot$ (from the Sun's barycenter)

[6] The French name standing for beach, because a plage resembles light-colored "sand" against the darker background.

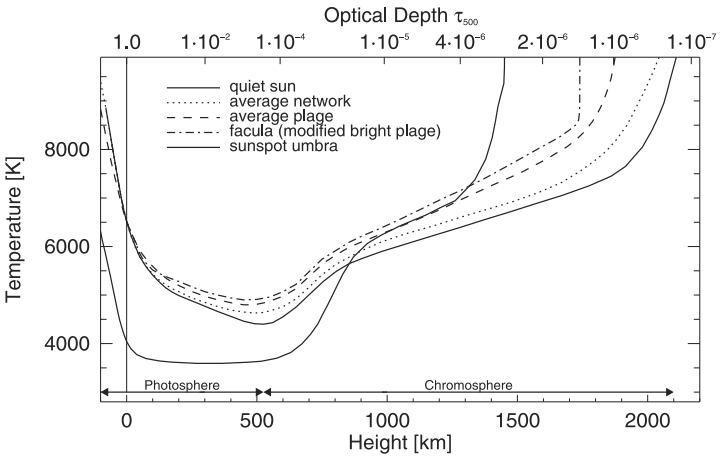

Fig. 2.6 Temperatures of solar magnetic regions *vs.* the height above the photosphere bottom. Height is defined in terms of the optical depth at 500 nm ($\tau_{500\ \mathrm{nm}} = 1$): the optical thickness at 500 nm and the corresponding distance in kilometers are shown (From [15], Courtesy of C. Fröhlich, PMOD, World Radiation Center, Switzerland)

such that $\tau(r_\odot) = 1$. This depends on the wavelength, of course. One can choose the wavelength of 500 nm (one of the standard lengths in Optometry), very close to the 501.34 nm of the wavelength maximum of a blackbody at 5780 K (from Wien's displacement law, or $\lambda_{max} T = 2.897768 \times 10^6$ nm K) and sufficiently close to the Sodium doublet 589/589.6 nm (i.e. energy separation of 0.0021 eV). The top of the photosphere corresponds to the minimum temperature of the *quiet* Sun as above defined. In Fig. 2.6, photosphere is "extended" about 100 km below in order to show how temperature increases rapidly. A "negative thick" solar shell of −40 km is radiation-accessible around 1.6 μm, where solar opacity achieves a minimum.

In the last years, a significant work has been carrying out for reconstructing TSI over the past centuries in the contest of Earth's climatology studies, especially between the end of the Maunder minimum to the present time. Since measurements of solar magnetic flux were not available before the second half of the 20th century, proxy quantities have been using, e.g. the records of the Zurich or group sunspot number, the sunspot area, the facular area, and the production rate of cosmogenic isotopes. Current models of TSI are shown to explain 90–95 percent of irradiance variability, at least with regard to reconstruction. An extended and excellent review can be found in [11].

Prediction of TSI exhibits additional difficulties. We limit ourselves to few considerations, some of which are oriented to solar sailing. Some models for explaining the various aspects of the solar activity and its time variations resort to what happens (or is supposed to happen) in the convection zone and tachocline. There, an electrically conducting fluid evolves under the action of the solar magnetic field that, in turn, is affected by this plasma. The solar field acts as the privileged channel of transport of energy to be ultimately released from the star. In order to describe

the *coupled* evolution of such field and matter (both exhibiting a broad spectrum of spatial/temporal scales), one has to use the equations of MHD.

—The following gray-box may be skipped on a first reading.—Put very simply, the magnetic field (if any) of a body with finite electric resistance would eventually decay if there were no internal source of electric field. Referring to celestial bodies, decay time is usually very brief compared to the body lifetime. If the body is observed to show persistent and/or cyclic magnetic fields, then some process has to be responsible for maintaining these fields. Such a process is named a *dynamo*, which acts against Ohmic losses. With regard to the Sun, there are various kinds of dynamo models aimed at explaining the solar cycles. Because the full MHD equations are extremely complicated, researchers are used to resort to reduced MHD equations; for instance, a family of dynamos is represented by the mean-field hydromagnetic models. In this set, the so-called *flux-transport* dynamos have been receiving considerable attention.

In a nutshell, according to the flux-transport dynamo models, the Sun should exhibit a complicated circulation, in the convective zone, symmetric with respect to the solar equatorial plane. If one cuts the solar sphere by a plane passing through the rotation axis, one may think of observing one of the four sections of the convective zone, as sketched in Fig. 2.7, where the Babcock-Leighton solar dynamo concept is illustrated. This is based on a special form of the magnetic field, as inferred from solar macroscopic features such as Hale's polarity law (which puts into evidence that solar cycle lasts 22 years), the sunspot *butterfly* diagram, synoptic magnetograms, and the shape of the solar corona during the minima of solar activity. As a result, the typical large-scale magnetic field in the convection zone (including the photosphere) may be pictured with two components: one longitudinal component and one component parallel to the local meridians; they are usually termed *toroidal* and *poloidal*, respectively.

According to Babcock-Leighton mechanism, the poloidal magnetic field, accumulated on the polar surface region-A at cycle n, will be moved down to the tachocline neighborhood; then, the toroidal field for cycle $n + 1$ can be produced along the path B–C. The magnetized plasma rises to region-D exhibiting a poloidal field again. A slow polarward surface motion, related to the new cycle, will follow. The characteristic times of such plasma movements are of considerable importance inasmuch as they may induce a chaotic behavior in the magnetic-field evolution, and this may be of great importance for the Earth's climate.

The previous considerations may be summarized by asserting that the Sun "remembers" its magnetic-field history; such memory intervenes in the cycle. If one takes the polarity of sunspots into account, the full basic solar cycle lasts about 22 years. A flux-transport dynamo model, also called the calibrated

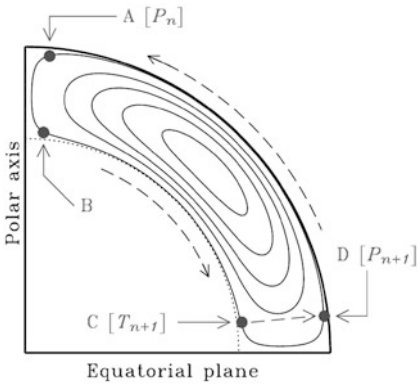

Fig. 2.7 Solar cycle model based on the Babcock-Leighton mechanism. The *closed lines* represent plasma streamlines on the solar meridian planes, known as the meridional circulation, inside the convective zone (From [8], courtesy of P. Charbonneau)

dynamo, has recently been setup including differential rotation (or the Ω-effect), Babcock-Leighton mechanism, meridional flow, and twisting/lifting of toroidal flux tubes (or the α-effect) on the surface and at the tachocline for regenerating poloidal fields. A model of such type (e.g. [10]) has been applied to the prediction of the cycle-24.

Very difficult is the problem of forecasting TSI. Figure 2.8 shows the evolution of the sunspot number from 2000, and the prediction for the current cycle-24. Thus, according to the Space Weather Prediction Center of National Oceanic and Atmospheric Administration (NOAA), maximum of sunspot number should occur in May 2013.

From the viewpoint of solar sailing, we have to stress some points:

1. The analysis of solar-cycle-related time series (in particular TSI) has not yet produced reliable predictions; some meaningful additional information is plainly required. However, for trajectory purposes, short-term proxy-based prediction might reveal to be sufficient for the guidance process. This point may represent an open research area for practical Solar-Photon Sailing (SPS).
2. Solar dynamo theories have been progressing considerably, but there is much to be done. Large-scale numerical simulations, supported by many additional data from solar-physics satellites, should eventually turn into results useful for SPS.
3. The time variations of the solar irradiance are described by means of the so-called *filling factors*, namely, the fraction of the solar surface covered by the elements (or components) of the model, e.g. sunspot umbrae, faculae, etc. Estimating such factors for each element represents a set of sub-problems to be solved. Quiet Sun's filling factor is the complement to unity of sunspots, faculae, or network.
4. TSI appears to exhibit several amplitude modulations. Some theoretical considerations suggest a superimposed chaotic behavior.

In Sect. 2.3, we will conceptually process the pieces of information of this section together with those of the following section devoted to spectral solar irradiance; the

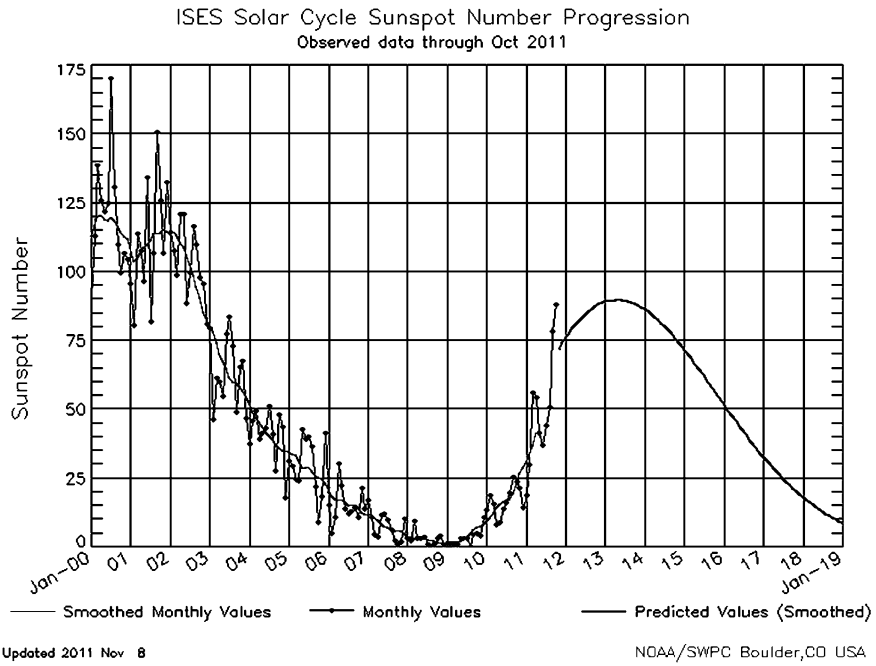

Fig. 2.8 Sunspot number evolution: observed and predicted values in November 2011. Courtesy of NOAA/SWPC

aim is to arrange a number of guidelines on the problem on how using the solar irradiance for a reliable in-space propellantless propulsion.

2.2.2 The Spectral Solar Irradiance

Total Solar Irradiance enters the thrust acceleration of any sailcraft directly (Chap. 6). Its relevance to solar sailing is therefore intuitive too. But also considerably important in designing a solar sail is the Spectral Solar Irradiance (SSI).[7] In order to show this in a simple way, let us recall the blackbody's main properties, which will be useful also to stress an important feature of the sailcraft thrust acceleration.

A blackbody is an ideal body absorbing electromagnetic radiation of every wavelength; it is in perfect thermodynamical equilibrium inside itself and with the ambient. Thus, it is also a perfect Lambertian emitter with spectral radiance $B(\lambda, T)$

[7]TSI represents the actual energy rate at the top of the Earth's atmosphere. Even SSI is notably important because, among various things, its large fluctuations in the UV band cause variations in the physical/chemical properties of the upper atmosphere.

depending only on wavelength λ and (absolute) temperature T:

$$B(\lambda, T) = \frac{2hc^2}{\lambda^5}\left[\exp\left(\frac{hc}{k}\frac{1}{\lambda T}\right) - 1\right]^{-1} \mathfrak{n}(\lambda)^2$$
$$= \left(\frac{1.03558434(4)\cdot 10^4}{\lambda}\right)^5\left[\exp\left(\frac{1.4387751(26)\cdot 10^7}{\lambda T}\right) - 1\right]^{-1}$$
$$\times\, \mathfrak{n}(\lambda)^2 \ \mathrm{W/(m^2\,nm\,sr)} \tag{2.22}$$

h and k denote Planck and Boltzmann constants, respectively. The figures in parentheses after the values represent one standard-deviation in the last corresponding digits. The second row of Eq. (2.22) can be plotted directly by inserting wavelength and temperature in (nm, K), respectively. $\mathfrak{n}(\lambda)$ is the index of refraction, at λ, of the medium surrounding the blackbody. For our practical purposes, we will set such quantity to unity for any wavelength. The blackbody radiance $B(T)$ and exitance $\mathcal{M}(T)$ are therefore given by

$$B(T) = \int_0^\infty B(\lambda, T)\,\mathrm{d}\lambda = \frac{2\pi^4 k^4}{15c^2h^3}T^4 \tag{2.23a}$$

$$\mathcal{M}(T) = \pi B(T) = \mathfrak{s}T^4 \tag{2.23b}$$

where $\mathfrak{s} = 5.670400(40) \times 10^{-8}\ \mathrm{W\,m^{-2}\,K^{-4}}$ is the Stefan–Boltzmann constant. Real bodies depart from the blackbody abstraction via different characteristics related to the complexity of the emitting surface; e.g. one can consider a celestial body endowed with variable atmosphere. In laboratory, there are very good realizations of the blackbody, or of the related concept known as the *hohlraum*, which is a cavity with the walls in thermal equilibrium with the inside radiant energy. A thermodynamical concept, which expresses any non-blackbody behavior in a simple way, is the *brightness* temperature. Suppose one has measured the spectral radiance, say, $\mathfrak{L}(\lambda)$ of some body in a certain wavelength range $[\lambda_1, \lambda_2]$; at a given λ_0 in this interval, there is *one* blackbody spectrum passing through the point $(\lambda_0, \mathfrak{L}(\lambda_0) \equiv \mathfrak{L}_0)$ in the $(\lambda, \mathfrak{L})$-plane. The corresponding temperature, the brightness one, can be easily obtained from the first row of Eq. (2.22). Denoting it by T_b, one gets

$$T_b(\lambda_0, \mathfrak{L}_0) = \frac{hc}{k\lambda_0}\left[\ln\left(1 + 2\frac{hc^2}{\lambda_0^5\mathfrak{L}_0}\right)\right]^{-1} \tag{2.24}$$

We will apply Eq. (2.24) here down.

Nowadays, via some professional distribution of solar-physics data, it is possible to download solar spectral irradiance data adjusted at 1 AU. Such adjustment is necessary because of the variable distance from the Sun of the solar instruments onboard Earth satellites, including those ones around the Lagrange point L1 of the Sun-Earth system. When one computes the solar brightness temperature distribution, one has to transform irradiance into radiance data multiplying the measured

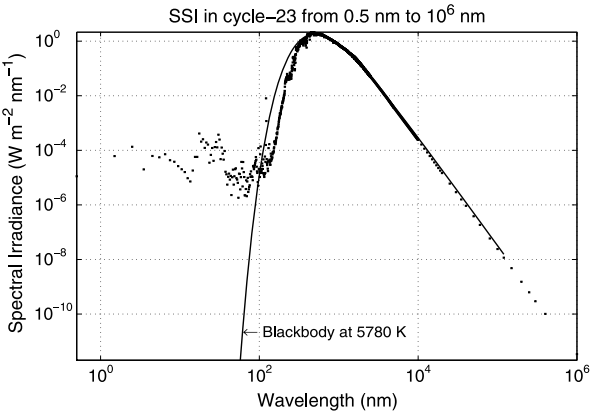

Fig. 2.9 The *dots* represent the solar spectral irradiance (daily data sets), averaged on all days of cycle-23, from 0.5 nm to 1 millimeter. The *solid line* is the irradiance at 1 AU caused by a blackbody with 5780 K

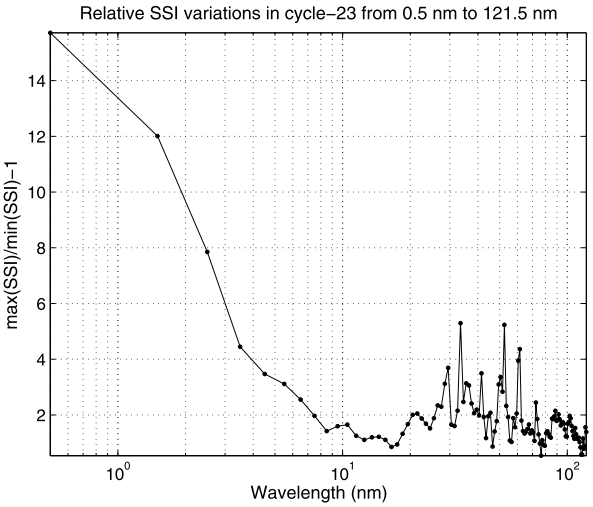

Fig. 2.10 Relative Changes in XUV/EUV irradiance during solar cycle-23: distribution is built by means of 1-nm bins. This 121-nm band is not covered by the ASTM-E490 tables

spectral irradiance by the factor $(\mathrm{AU}/r_\odot)^2/\pi \cong 214.9^2/\pi$, which entails a quasi point-like Sun (an apt assumption in the context of this chapter). Of course, the reciprocal of this number has to be used in transforming radiance to irradiance.

Figures 2.9 and 2.10 regard SSI in cycle-23. We have processed these solar irradiance data provided by Space Environment Technologies, CA, [38, 39].

In Fig. 2.9, dots represent daily data sets, averaged on all days of cycle-23, from 0.5 nm to 10^6 nm. (The current solar cycle is 24). The solid line is the irradiance

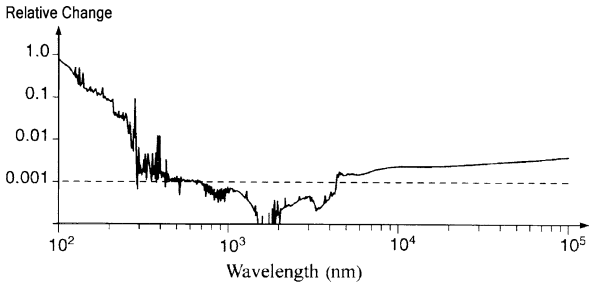

Fig. 2.11 Solar spectral variations over a solar cycle in the 100–100,000 nm broadband. A further finer structure, i.e. a higher resolution SSI in this band should not concern fast solar sailing. Adapted from [34], courtesy of Springer

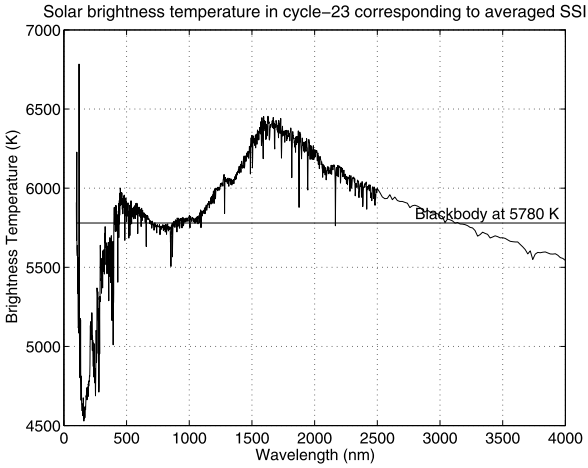

Fig. 2.12 Profile of the Sun's brightness temperature in cycle-23. Temperatures correspond to the means of SSI shown in Fig. 2.9; the reported band has been limited to 100–4,000 nm

at 1AU caused by a fictitious solar blackbody with 5780K. Roughly, the Sun looks like such a blackbody; however, SSI departs quite impressively from the ideal emitter in the EUV band down to the soft X-ray wavelengths (XUV). Not only, but these bands exhibit strong variations during the solar cycle, as shown in Fig. 2.10, where we plotted the relative change max(SSI)/min(SSI)-1 as function of the wavelength in 1-nm bins. This 121-nm band is not included in the E490 tables from American Society for Testing and Materials (ASTM), as documented in [3]. In particular, in the XUV region, changes are very strong. This situation has not been characteristic of cycle-23 only. As a point of fact, Fig. 2.11 shows SSI typical change over solar cycle in the 100–100,000 nm broadband. In the visible band and beyond up to the thermal and far infrared region (FIR), variations are negligible. In contrast, as wavelength goes below the visible region, fluctuations increase considerably. This is quite important, in particular, for the chemical-physical properties of the terrestrial thermosphere/ionosphere.

Figure 2.12 shows the brightness temperature profile for the spectral irradiance of cycle-23. The horizontal line refers to the 5780 K blackbody, which is crossed by the brightness temperature profile in a small number of points. Finally, in Fig. 2.13 we plotted the $\int_{0.5\text{ nm}}^{\lambda} \mathcal{I}(\ell)\,\mathrm{d}\ell$, namely, the mean SSI (shown in Fig. 2.9) integrated over wavelength. With regard to the visible region, different definitions are found in

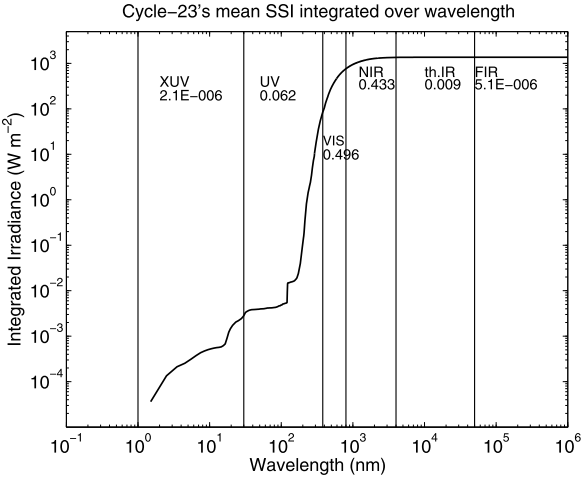

Fig. 2.13 SSI integrated over wavelength. Shown are the main electromagnetic bands, bounded by vertical lines, and their related fractions of TSI

literature (with different justifications). We have adopted the 380–800 nm band in Fig. 2.13, namely, the interval of wavelength of the spectral sensitivity of the human eye, which includes both the photopic and the scotopic visions. CIE has defined the spectral luminous efficiency functions relatively to this range.

Though we detailed cycle-23 only, the following considerations regard solar sails in general:

1. Approximately 99 percent of TSI falls in the 200–4000 nm range; this is important since the thickness of most of the all-metal solar sails already studied for fast sailing is close to 100 nm.
2. The UV-fraction of TSI might appear negligible; however, it amounts to about 48 times (at least) the full TSI relative fluctuations in a cycle, and we shall analyze the impact of the variable TSI on fast sailcraft trajectories.
3. UV photons may also have a cumulative effect on trajectory by altering the reflective layer of the sail (at least, with regard to sails conventionally conceived).
4. XUV and FIR bands do not seem to be a problem as long as the sailcraft does not spend much time very close to the Sun.

2.3 Principles of Utilization of Sunlight for in-Space Propulsion

Since the first half of the 20th century, sunlight has been taking seriously as the basic external source of momentum flux for non-rocket spacecraft. In particular, Tsiolkovsky and Zander wrote explicitly that very thin sheets, pushed by the sunlight pressure, should be able to achieve high speeds in Space. Garwin coined the term *solar sailing* [17]. From what discussed in Sects. 2.2.1 and 2.2.2, in particular

at the end of those sections, it is possible arrange a number of items oriented to solar sailing. Sun releases plenty of energy per unit time. This is in form of photons, particles, and magnetic fields filling the heliosphere. Emission can be either continuous (e.g. the normal sunlight and solar wind) or time-localized (e.g. flares and coronal mass ejection); of course, *continuous* does not mean constant in any case. Also, ejection of matter and energy may involve a large fraction the whole solar surface, or be space-localized. When a space mission of any kind is designed, there is an implicit basic assumption that a mission planner/designer makes: the trajectory/orbit of the spacecraft has to be computable in essentially deterministic way. This does not mean that transfer trajectories and operational orbits—including any maneuvers—are free of uncertainties. Fatal errors may happen in delicate mission phases because something goes wrong, of course. In contrast, uncertainties come from sources of errors such as inadequate force field models, insufficient knowledge of relevant parameters, noised measurements of the observables, intrinsic fluctuations of engines, biases in numerical methods for propagating the spacecraft state, and so forth. The spacecraft state evolution with control and stochastic noise is the general problem to be dealt with in a real space mission. In all cases, however, one is confident that things (apart from accidents and/or quite unknown situations unforeseeable in advance) go sufficiently close to what calculated in the design phase and/or updated in the course of flight as soon as measurements (from ground and/or spacecraft instruments) become available.

The design and construction of space rocket engines have become highly accurate and reliable; so are the navigation, guidance and control processes. Now, if we want to use a non-rocket propulsion for many advanced missions, especially those ones impossible for any practical rockets, the first thing to do is to search for an external source of power *sufficiently* intense, stationary, and predictable. Let us discuss these three items, in the order, applied to the Sun. If one wants to utilize sunlight for space propulsion, there are two general options: (1) to absorb solar power and transfer it to some *onboard* reaction mass which shall be ejected, (2) to transform the radiation pressure into a force acting on the spacecraft.

The first option resembles a rocket, although conceptually it is not; such spacecraft does not need a primary source of power onboard, and this represents a strong advantage. Nevertheless, because some matter has to be ejected for getting thrust, we would go back to the problems of mass characterizing rocket spacecraft.

The second option entails that the electromagnetic radiation has to interact with some material surface, or the sail, in order to get a propulsive acceleration. This sail can be well approximated with a two-dimensional (more or less curved) surface with a supporting subsystem. Thus, the utilization of TSI appears natural, even though not so obvious as one might think because of the properties of SSI. We have to search for a low-density material, mechanically and thermally apt to be extended, and long-lasting thin space films operating in a wide range of distances from the Sun, and optically reflecting at least in the range 200–4,000 nm. This range is a good reference band; however, in the next chapters, we will considered different values in dealing with specific effects.

One needs an external source with a particular feature, namely, a sufficient *predictability*; it deserves special attention. In general, a propulsion concept based on

a highly unpredictable, though existing, power source may turn into an unmanageable space system. A good policy should be to resort to a novel propulsion system that can solve the unsurmountable problems of the old one *without* introducing new big problems. Said differently, the novel system should to be able to deliver payloads at new targets, unrealistic for the old propulsion, with the desired accuracy and precision.

As it is known, mission success relies on high-quality spacecraft/mission design, including the processes of navigation, guidance and control. Nevertheless, a manageable flight depend primarily on the features of the momentum flux source. Let us clarify this point by means of an example. Suppose we want to design a sailcraft leaving some high Earth orbit for reaching Mars, putting the payload on the desired orbit about the planet, and going back to the departure orbit about the Earth. Suppose that the sailcraft will be launched in December 2019, and that the design of the transfer trajectory begins in January 2015. The envisaged flight should then start around the minimum between cycles 24/25 (if cycle-24 lasts 11 years). During the feasibility analysis of the flight design, assuming that the Earth-to-Mars arc and the Mars-to-Earth arc may last about one year each, it is reasonable to use the mean value of TSI throughout 2007 and 2008, respectively, in the trajectory calculations (see Figs. 2.4 and 2.8). For cycle-24, there is a non-negligible uncertainty about its maximum. For cycle-25, nobody knows today, even though a profile similar to that of cycle-24 appears a reasonable starting point. In any case, in the subsequent phases of the design, calculations should be refined by considering different levels of TSI; eventually, more appropriate TSI data—related to the time interval of the *real* flight—will have to be input to the mission analysis codes. Periodically updating the solar database via onboard measurements may be one of the key-points in designing sophisticated sailcraft missions.

One expects that high-frequency changes of TSI should not affect trajectory because of sailcraft inertia, whereas too smoothed TSI data should introduce some target missing higher than some prefixed mission-dependent tolerance(s). After the launch is performed, the actual solar irradiance the sailcraft will receive during its flight is not known deterministically. In Sect. 9.1, we will preliminarily analyze TSI-variable trajectories. This solar variability may be considered as consisting of three components: one is a secular trend, the second one regards cyclic changes, whereas the third one might be represented by stochastic fluctuations.

- What renders SPS attractive, even from this point of view, is the combination of the small amplitude (about 0.15 percent) of the TSI fluctuations about the mean (see also Fig. 3.10), and the long-period high spectral power, as Fig. 2.14 shows very clearly.
- Space sails will have to be controlled, of course. This should be possible with no insurmountable difficulty essentially because solar sail is just two dimensional, not a large volume that would act as a "reflecting sail". Nevertheless—since the TSI thrust acceleration can be continuous

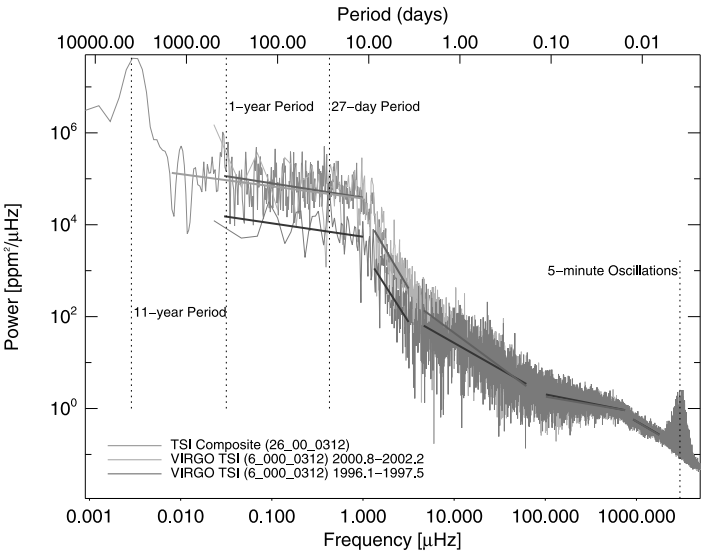

Fig. 2.14 Total Solar Irradiance in the frequency domain via Fourier analysis. Period is from 1978 to 2002. Temporal scales from few minutes to a solar cycle are evident. The 1996–1997 spectrum includes the minimum between cycles 22/23. The 2000–2002 spectrum pertains to high solar activity in cycle-23. Fourier-processed data come from SOHO/VIRGO radiometer system (From [15], courtesy of C. Fröhlich, PMOD, World Radiation Center, Switzerland)

for many years—controlling, stabilizing and maneuvering a structure by far surpassing in size all other sailcraft systems represents one of the key points to manage in order to guide a sailcraft exactly as one wants.

Considering TSI fluctuations is one way of computing sailcraft trajectories; in Chap. 9, we will show that such time variations may cause deviations of sailcraft trajectories, if not dealt with in the flight design.

Either spin-stabilized or three-axis stabilized sail control may be appropriate, depending on the mission. The meaningful point is that—among the propellantless attitude control methods—TSI could be utilized even for attitude control especially when sailcraft draws close to the Sun in future missions. IKAROS inaugurated this method successfully.

References

1. Abbot, C. G. (1911), The Sun. New York: Appleton and Company. Read online at http://www.archive.org/stream/thesunab00abbouoft#page/n7/mode/2up.

2. Abbot, C. G. (1966), Solar variation, a weather element. Proceedings of the National Academy of Sciences of the United States of America, 56(6).
3. ASTM International (2006), Standard Solar Constant and Zero Air Mass Solar Spectral Irradiance Tables, E490, 16 pages, PA 19428-2959, USA.
4. Bennet, J. M., Mattsson, L. (1999), Introduction to Surface Roughness and Scattering (2nd edn.). New York: Optical Society of America.
5. Berrilli, F., Del Moro, D., Viticchiè (2008), Magnetic field distribution in the quiet Sun: a simplified model approach. Astronomy and Astrophysics manuscript No. 9683aph, August 4th.
6. Calisesi, Y., Bonnet, R.-M., Gray, L., Langen, J., Lockwood, M. (Eds.) (2007), Solar Variability and Planetary Climates. Berlin: Springer. ISBN 978-0-387-48339-9.
7. Charbonneau, P. (2007), Flux transport dynamos. Scholarpedia, 2(9), 3440.
8. Charbonneau, P. (2005), Dynamo models of the solar cycle. Living Reviews in Solar Physics.
9. Dikpati, M. (2005), Large scale organization in the solar dynamo and its observational signature. Astronomical Society of the Pacific, 346, 61–76.
10. Dikpati, M., De Toma, G., Gilman, P. A. (2006), Predicting the strength of solar cycle 24 using a flux-transport dynamo-based tool. Geophysical Research Letters, 33, L05102.
11. Domingo, V., Ermolli, I., Fox, P., Fröhlich, C., Haberreiter, M., Krivova, N., Kopp, G., Schmutz, W., Solanki, S. K., Spruit, H. C., Unruh, Y., Vögler, A. (2009), Solar surface magnetism and irradiance on time scales from days to the 11-year cycle. Space Science Reviews, 145, 337–380. doi:10.1007/s11214-009-9562-1.
12. Foster, S. S. (2004), Reconstruction of solar irradiance variations for use in studies of global climate change. Ph.D. dissertation at University of Southampton, School of Physics and Astronomy. ftp://ftp.pmodwrc.ch/pub/Claus/Publications/.
13. Fox, M. (2007), Oxford Master Series in Physics: Quantum Optics, an Introduction. Oxford: Oxford University Press. ISBN 978-0-19-856673-1.
14. Fröhlich, C. (2004), Solar energy flux variations. In Solar Irradiance Variability, Geophysical Monograph: Vol. 141. Solar Variability and Its Effect on Climate (pp. 97–110). Washington: American Geophysical Union.
15. Fröhlich, C., Lean, J. (2004), Solar radiative output and its variability: evidence and mechanisms. The Astronomy and Astrophysics Review, 12, 273–320. doi:10.1007/s00159-004-0024-1.
16. Fröhlich, C. (2006). Solar Irradiance Variability Since 1978, Space Science Review. Dordrecht: Kluwer Academic.
17. Garwin, R. L. (1958), Solar sailing: a practical method of propulsion within the solar system. Jet Propulsion, 28, 188–190.
18. Golub, L., Pasachoff, J. M. (2002), Nearest Star: The Surprising Science of Our Sun, Harvard: Harvard University Press. ISBN 0-674-01006-X.
19. Hathaway, D. H., Wilson, R. M. (2006), Geophysical Research Letters, 33, L18101.
20. Hoyt, D. V., Kenneth, H. Schatten (1997), The Role of the Sun in Climate Change. Oxford: Oxford University Press.
21. Krivova, N. A., Balmaceda, L., Solanki, S. K. (2007), Reconstruction of total solar irradiance since 1700 from the surface magnetic flux. Astronomy & Astrophysics, 467, 335–346.
22. Krivova, N. A., Solanki, S. K., Floyd, L. (2006), Reconstruction of solar UV irradiance in cycle 23. Astronomy & Astrophysics, 452, 631–639.
23. Krivova, N. A., Solanki, S. K. (2005), Modelling of irradiance variations through atmosphere models. Memorie Della Societa Astronomica Italiana, 76, 834–841.
24. Lockwood, M. (2002), An evaluation of the correlation between open solar flux and total solar irradiance. Astronomy & Astrophysics, 382, 678–687.
25. Mekaoui, S., Dewitte, S. (2008), Total solar irradiance and modelling during cycle 23, Solar Physics, 247, 203–216. doi:10.1007/s11207-007-9070-y.
26. NASA/MSFC Solar Group (2008), http://solarscience.msfc.nasa.gov/papers.shtml (a set of downloadable PDF-format papers), http://solarscience.msfc.nasa.gov/presentations.shtml (a set of downloadable .avi and .ppt-format presentations).
27. NASA, Solar Dynamics Observatory (SDO), http://sdo.gsfc.nasa.gov/.

28. NASA, Solar Heliosperic Observatory (SOHO), http://sohowww.nascom.nasa.gov/.
29. Space Weather Prediction Center, http://www.swpc.noaa.gov/index.html.
30. Solanki, S. K., Krivova, N. A., Wenzler, T. (2004), Irradiance models. Advances in Space Research, 35, 376–383.
31. Solanki, S. K., Krivova, N. A. (2005), Solar variability of possible relevance for planetary climates. Space Science Reviews, 125, 25–37.
32. Wei-Hock, Soon W., Yaskell, S. H. (2003), The Maunder Minimum and the Variable Sun-Earth Connection. Singapore: World Scientific. ISBN 981-238-275-5.
33. Parr, A. (2005), Experimental Methods in the Physical Sciences: Vol. 41. Optical Radiometry. New York: Academic Press.
34. Rozelot, J. P. (Ed.) (2006), Lecture Notes in Physics: Vol. 699. Solar and Heliospheric Origins of Space Weather. Berlin: Springer. ISBN 3-540-33758-X, ISSN 0075-8450.
35. Rozelot, J. P., Neiner, C. (Ed.) (2008), Lecture Notes in Physics: Vol. 765. The Rotation of Sun and Stars. Berlin: Springer. ISBN 3-540-878300
36. Schatzman, E., Praderie, F. (1990), The Stars. Berlin: Springer. Translator King, A. R. ISBN 3-540-54196-9.
37. Wolfe, W. L. (1998), SPIE Tutorial Texts in Optical Engineering: Vol. 29. Introduction to Radiometry.
38. Tobiska, W. K., et al. (2000–2008), http://www.SpaceWx.com, many downloadable papers.
39. Solar Irradiance Platform (professional grade) (2009), Space Environment Technologies, version 2.35, http://www.SpaceWx.com.
40. Wenzler, T., Solanki, S. K., Krivova, N. A., Fröhlich, C. (2006), Reconstruction of solar irradiance variations in cycles 21–23 based on surface magnetic fields. Astronomy & Astrophysics, 460, 583–595.

http://www.springer.com/978-94-007-4776-0

Fast Solar Sailing
Astrodynamics of Special Sailcraft Trajectories
Vulpetti, G.
2013, XXX, 410 p., Hardcover
ISBN: 978-94-007-4776-0